Korean J. Chem. Eng., 37(1), 93-104 (2020)
DOI: 10.1007/s11814-019-0411-y

pISSN: 0256-1115
eISSN: 1975-7220

Application of amine-functioned Fe_3O_4 nanoparticles with HPEI for effective humic acid removal from aqueous solution: Modeling and optimization

Seyedeh Mahtab Pormazar*,, Mohammad Hassan Ehrampoush*, Mohammad Taghi Ghaneian*, Mehdi Khoobi***,****, Parvaneh Talebi*, and Arash Dalvand*,†**

*Environmental Science and Technology Research Center, Department of Environmental Health Engineering, School of Public Health, Shahid Sadoughi University of Medical Sciences, Yazd, Iran
**Student Research Committee, Shahid Sadoughi University of Medical Sciences, Yazd, Iran
***Biomaterials Group, The Institute of Pharmaceutical Sciences (TIPS), Tehran University of Medical Sciences, Tehran 1417614411, Iran
****Department of Pharmaceutical Biomaterials and Medicinal Biomaterials Research Center, Faculty of Pharmacy, Tehran University of Medical Sciences, Tehran, Iran
(*Received 24 July 2019 • accepted 15 October 2019*)

Abstract−Humic acids are one type of natural organic matter and precursors of chloro organic compounds that cause a major problematic issue for water treatment plants. In the present study, Hyperbranched polyethylenimine (HPEI) was grafted onto Fe_3O_4 nanoparticles for HA adsorption from aqueous solution. Fe_3O_4@HPEI nanoparticles were characterized via TEM, SEM, FTIR, XRD, VSM, and BET analysis. The effects of various operational parameters including initial HA concentration, pH, adsorbent dose, contact time and ionic strength on the HA removal were assessed. According to the obtained statistical model, the optimal condition was acquired at the initial HA concentration 79 mg/L, adsorbent dose 0.128 g/L, pH 3 and contact time 29 min, which up to 97.27% HA were adsorbed by Fe_3O_4@HPEI that was close to the predicted result by the model (95.6%) that confirmed the validity of the selected model. The adsorption data were fitted to the pseudo-second-order kinetic and Freundlich isotherm. Thermodynamic parameters indicated that the adsorption process was spontaneous and endothermic. The fabricated Fe_3O_4@HPEI nanoparticles could be repeatedly utilized as a suitable adsorbent to remove HA from the aqueous environment.

Keywords: Box-Behnken Design, Fe_3O_4@HPEI, Humic Acid Adsorption, Modeling

INTRODUCTION

Humic acids (HA) are complex macromolecules and one type of natural organic matter (NOM) that exist in soil and sources of drinking water supply [1,2]. They are a very complex combination, so cannot be illustrated by any single formula; however, $C_{187}H_{186}O_{89}N_9S$ is a common chemical formula for humic acid [3,4]. HA carry net negative charges, resulting from the variety of different functional groups such as carboxylic (-COOH) and phenolic (-OH) which attached to aromatic rings [5].

HA is insoluble in water under strongly acidic conditions but dissolves at pH above 2 (pH>2) [6]. Approximately 40-90% of dissolved organic matter found in the fresh water supply may be attributed to this compound [5]. HA concentration in underground and surface water ranges widely from 20 μg/L to 30 mg/L, respectively [7]. HA in water can cause brown or yellow color, taste, odor, and be a serious problem for aquatic organisms [8]. Furthermore, in conventional drinking water treatment, HA reacts with chlorine and produces disinfection by-products (DBPs), like trihalomethanes (THMs) [9] and haloacetic acids (HAAs), haloacetonitriles, haloketones, trichloronitromethane and trichloroacetaldehyde, which are a potential precursor to carcinogenic [3,10]. Therefore, it is necessary to find effective methods for removing HA from the water. Various techniques have been used to minimize the concentration of HA in aqueous solution, for instance, coagulation [11], electrocoagulation [12], advanced oxidation [13], ultrafiltration [14] and adsorption. Among these, adsorption has been generally considered because it has easy operation, simple design, high efficiency, and low investment [15].

In the past decades, magnetic nanoparticles have gained special attention in water purification due to their high extraction efficiency, simple manipulation process, large surface area, strong adsorption ability, easily separated from water and easy recovery [16,17]. One of the most commonly used magnetic materials is Fe_3O_4 nanoparticles that have been used in many areas, like biotechnology, biomedical, environmental remediation and wastewater treatment [18,19]. However, magnetic nanoparticles (Fe_3O_4) have some limitations, as they form aggregations in aqueous solutions due to strong magnetic dipole-dipole attractions between particles and so lose their ability to remove the pollution [17,20]. In addition, magnetite is not stable and could be oxidized, which alters its magnetic properties [21]. Thus, it is necessary to modify the surface of magnetic nanoparticles not only to solve these problems but also to enhance nanoparticle capacity and improve their efficiency [22]. For this purpose,

†To whom correspondence should be addressed.
E-mail: arash.dalvand@gmail.com

magnetic nanoparticles have been modified with different amino acids compounds like arginine [23], cysteine [17], lysine [24] and guanidine [25].

Recently, the application of modified magnetic nanoparticles in HA removal has been studied. Kumari et al. used polyethylene glycol (PEG) for surface modification of Fe_3O_4 and its efficiency in HA removal was investigated [26]. Fe_3O_4-chitosan hybrid nanoparticles were prepared by Zulfikar et al. and successfully used to remove HA [5].

Hyperbranched polyethylenimine (HPEI) is a macromolecular polyamine containing a large number of primary, secondary and tertiary amine functional groups on its molecular chains [27]. In addition, PEI has a high positive charge density in a broad pH range, which makes it very useful in the functionalization of Fe_3O_4 nanoparticles to adsorb negatively charged analytes [28,29].

In the present work, HPEI was grafted onto Fe_3O_4 nanoparticles to improve the performance of HA removal from the aqueous environment. The efficiency of fabricated Fe_3O_4@HPEI for adsorption HA was studied and an appropriate model was suggested to determine the optimum value of various operational parameters and obtaining favorable conditions.

MATERIALS AND METHODS

1. Materials

Humic acid sodium salt 50%, hyperbranched polyethylenimine (HPEI, molecular weight: 60,000 g/mol, 50 wt% in H_2O), and [3-(2, 3-Epoxypropoxy)-propyl]-trimethoxysilane (EPO, 98%) were prepared from Sigma-Aldrich. $FeSO_4{\cdot}7H_2O$, $FeCl_3{\cdot}6H_2O$ (Grade: ACS, ISO, Reag. Ph Eur), ammonia solution (NH_4OH, 25%), sodium hydroxide (NaOH), Hydrochloric acid (HCL, 98%) and toluene were obtained from Merck.

2. Synthesis of Fe_3O_4 Nanoparticles

Magnetic nanoparticles (Fe_3O_4) were prepared by chemical co-precipitation method. 0.7 g $FeSO_4{\cdot}7H_2O$ and 1.17 g $FeCl_3{\cdot}6H_2O$ were added into 50 mL deionized water and stirred for 30 min under nitrogen gas at 70 °C. Then, 10 mL NH_4OH (25%) was dropped slowly into the mixture and stirred for 1 hour. The Fe_3O_4 nanoparticles were segregated by an external magnet. The product was washed five times with water and dried in an oven at 50 °C for 24 hours.

3. Synthesis Fe_3O_4@HPEI Nanoparticles

1 g of HPEI was poured into 200 mL dry toluene and 0.4 g EPO was dropped slowly in the reaction mixture and agitated for 24 hours at 80 °C. Then 1 g prepared Fe_3O_4 nanoparticles were dispersed in 25 mL ethanol and added in the above reaction mixture, stirring continued for 24 hours at 80 °C. The obtained black powder was separated by an external magnet and washed several times with ethanol. Finally, it was dried in vacuum for 24 hours [30]. The synthesis process is schematically illustrated in Fig. 1.

4. Characterization of Adsorbent

Imaging and examining the microscopic structure of magnetic nanoparticles were carried out via field emission scanning electron microscope (FE-SEM) and transmission electron microscopy (TEM) (EM10C-100 KV, Zeiss Co, Germany). Fourier transform infrared spectroscopy (FTIR) (Spectrum Two, PerkinElmer Co) was used to achieve infrared spectrum of the adsorbent. For identification phase of crystalline structures, X-ray diffraction (XRD) (X' Pert Pro, PANalytical Co, Netherlands) was utilized. In addition, magnetic property through vibrating sample magnetometer (VSM)

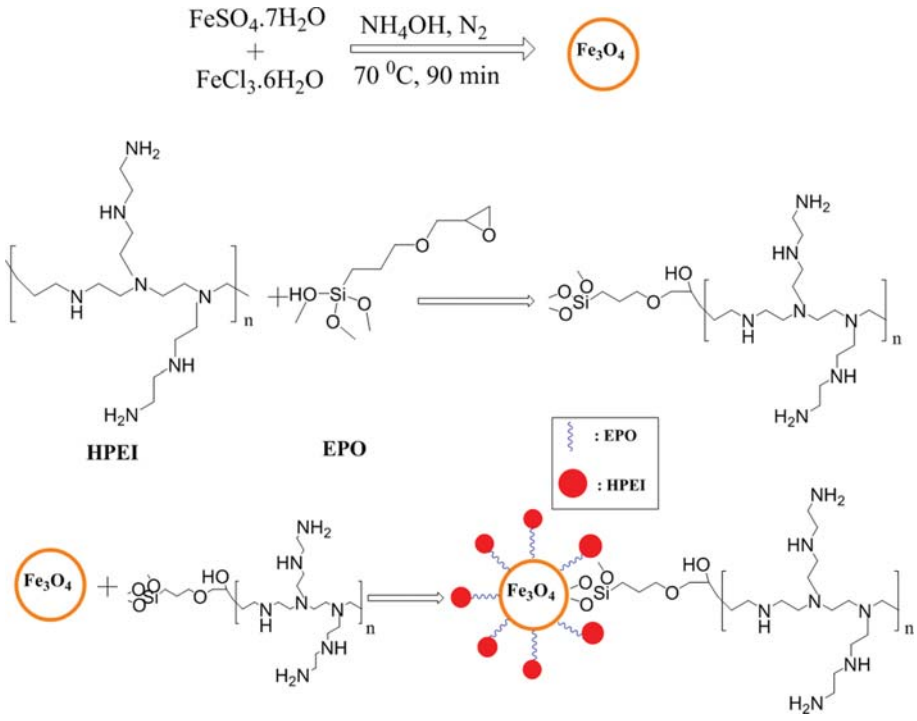

Fig. 1. Synthesis procedure of Fe_3O_4@HPEI nanoparticles.

(Meghnatis Daghigh Kavir Co, Iran) was determined, and the specific surface area was measured by Brunauer-Emmett-Teller's test (BET) (Nova, Quantachrome CO, USA).

5. Preparation of Stock Solution of Humic Acid

HA stock solution was prepared by dissolving 0.5 g of HA in 1,000 mL NaOH solution (0.01 mol/L) and stirring for 24 hours. Then, the solution was filtered through a 0.45 μm membrane filter (cellulose acetate). The HA stock solution was stored in a dark place and at 4 °C [31]. Solutions of the desired HA concentrations for the experiments were obtained by diluting the stock solution.

6. Adsorption Experiments

All experiments were performed in 50-mL Erlenmeyer flask containing 25 mL HA solution with a predetermined dose of Fe_3O_4@HPEI nanoparticles added. The pH was adjusted with NaOH (0.1 M) and HCl (0.1 M). Samples were shaken at 200 rpm during different contact time, and then the adsorbent was separated by a magnet. The concentration of HA before and after adsorption was measured with UV-VIS spectrophotometer (HACH DR-6000, USA) at 254 nm wavelength. The removal efficiency and the adsorption capacity [32,33] of the HA were determined by Eqs. (1) and (2):

$$E(\%) = \frac{C_0 - C_e}{C_0} \times 100 \quad (1)$$

Table 1. Range of the input variables with their levels for HA adsorption on Fe_3O_4@HPEI nanoparticles

Parameter	Unit	Code	Parameters levels		
			−1	0	1
HA concentration	mg/L	A	10	55	100
pH	-	B	3	6	9
Contact time	min	C	2	16	30
Adsorbent dose	g/L	D	0.04	0.17	0.3

$$q_e = \frac{(C_0 - C_e)V}{m} \quad (2)$$

where, C_0 (mg/L), C_e (mg/L), q_e (mg/g), m (g), and V (L) are the initial concentration of the HA, the equilibrium concentration of the HA, the adsorption capacity (HA adsorbed onto the Fe_3O_4@HPEI nanoparticles), the adsorbent mass and the solution volume, respectively [34].

7. Design of Experiments

The effects of various operational parameters including initial HA concentration (10, 55 and 100 mg/L), adsorbent dose (0.04, 0.17 and 0.3 g/L), pH (3, 6 and 9), and contact time (2, 16 and 30 min)

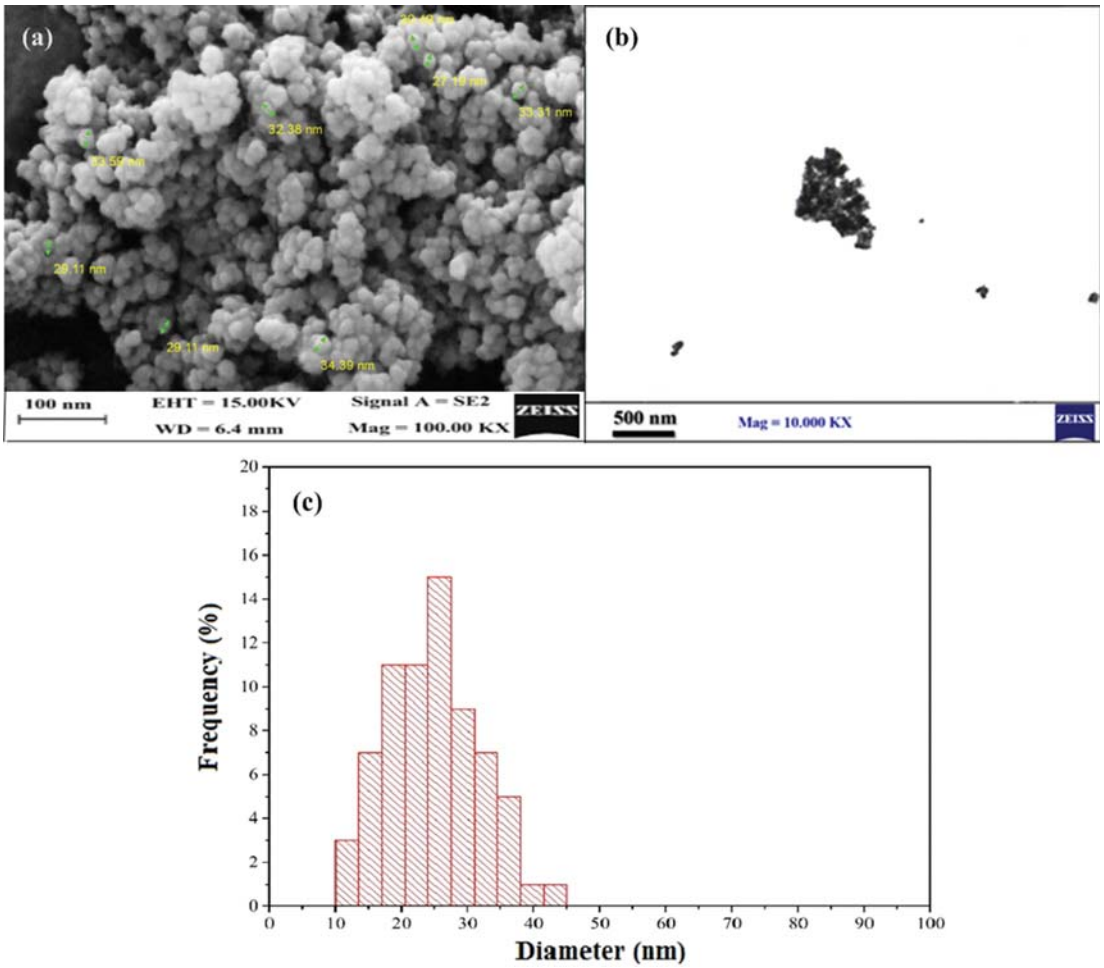

Fig. 2. (a) FE-SEM, (b) TEM image, and (c) histogram plot of Fe_3O_4@HPEI nanoparticles.

on the HA removal by Fe_3O_4@HPEI nanoparticles were assessed.

Designing the model and analyzing experimental data involved using the Design Expert software (version 7, trial, Stat-Ease). Box-Behnken design was applied for response surface methodology. In Table 1, the operational ranges of input variables with their coded levels and also real units of variables are displayed. The response variable was fitted to a second-order polynomial model for predicting the optimal conditions in HA adsorption process. The second-order polynomial model can be expressed by Eq. (3) [35,36].

$$Y = \beta_0 + \Sigma_{i=1}^{K} \beta_i \cdot X_i + \Sigma_{i=1}^{K} \beta_{ii} \cdot X_i^2 + \Sigma_{i=1}^{K} \Sigma_{j=1}^{K} \beta_{ii} \cdot X_i \cdot X_j + \varepsilon \quad (3)$$

where Y represents the predicted response (the percent of HA removal), β_0 is the constant coefficient, β_i, β_{ii}, β_{ij} represent the linear, quadratic and interaction coefficients, respectively; x_i or x_j are the variables. k and ε are the number of factors studied and the random error, respectively [37].

RESULTS AND DISCUSSION

1. TEM and FE-SEM Analysis

The morphology of the Fe_3O_4@HPEI nanoparticles was characterized by field emission scanning electron microscope (FE-SEM) and transmission electron microscope (TEM), and the results are represented in Fig. 2. As shown in this figure, the nanoparticles had a spherical shape. According to the histogram plot, the size of synthesized Fe_3O_4@HPEI nanoparticles was in the range of 10 to 45 nm. The results confirmed that Fe_3O_4@HPEI nanoparticles were at nano-size scale.

2. X-ray Diffraction (XRD)

X-ray diffractometry (XRD) was used to examine the crystal structure and integrity of the magnetic particles incorporated HPEI. The XRD pattern of Fe_3O_4@HPEI is illustrated in Fig. 3. It can be easily observed that the sharp peaks at 2θ: 30.1° (220), 35.5° (311), 43.1° (400), 53.7° (422), 57.1° (511), 62.6° (440), and 74.9° (533) matched the diffraction peaks of the pure Fe_3O_4 (JCPDS No. 19-0629) magnetic nanoparticles [38]. The characteristic peaks of Fe_3O_4 were observed, indicating that Fe_3O_4 was present into the Fe_3O_4@HPEI. Similar diffraction peaks for Fe_3O_4 functionalized with polyethylenimine were reported by the Chen et al. [28].

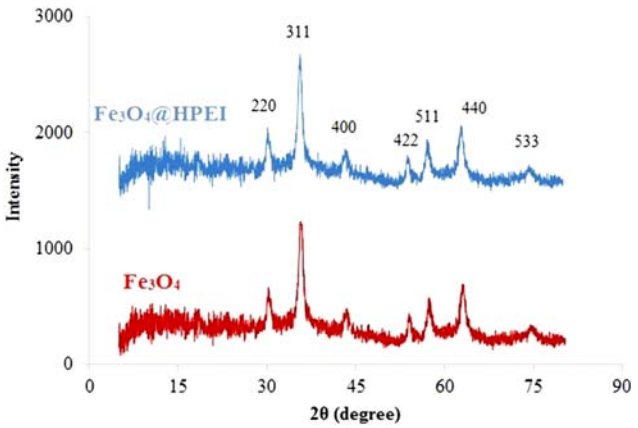

Fig. 3. The XRD pattern of the Fe_3O_4@HPEI nanoparticles.

3. FTIR

FTIR analysis was used to confirm that HPEI were successfully grafted on the Fe_3O_4 nanoparticles. The FTIR spectra of Fe_3O_4 and Fe_3O_4@HPEI nanoparticles are illustrated in Fig. 4. The absorption peaks at 625 and 628 cm^{-1} correspond to the stretching vibration of the Fe-O, assigned to the magnetite phase. Also O-H stretching vibration at 3,405 cm^{-1} band was found for the Fe_3O_4 nanoparticles. For Fe_3O_4@HPEI, The stronger peak at 3,448 cm^{-1} was ascribed to N-H stretching that demonstrated amino functional groups formed on the surface of nanoparticles. The intensity observed at 2,971 cm^{-1} and 2,893 cm^{-1} was ascribed to C-H bands, and the peaks at 1,645 cm^{-1} and 1,389 cm^{-1} are attributed to the stretching vibration of C-C. The Si-O-H and Si-O-Si stretching appear at about 1,000 cm^{-1} and 1,121 cm^{-1}.

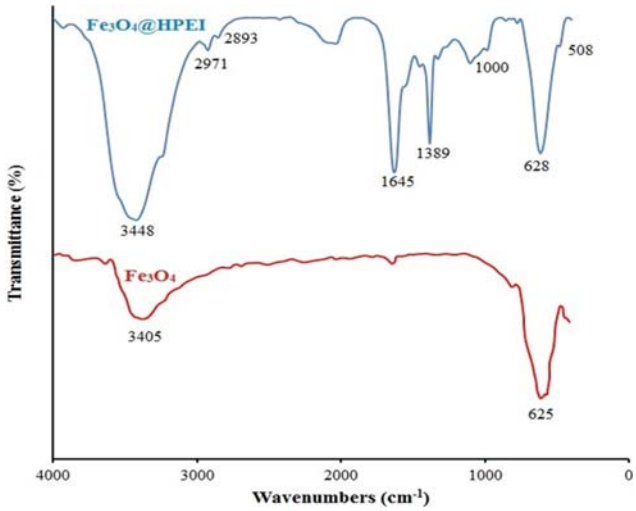

Fig. 4. FTIR spectra of Fe_3O_4@HPEI nanoparticles.

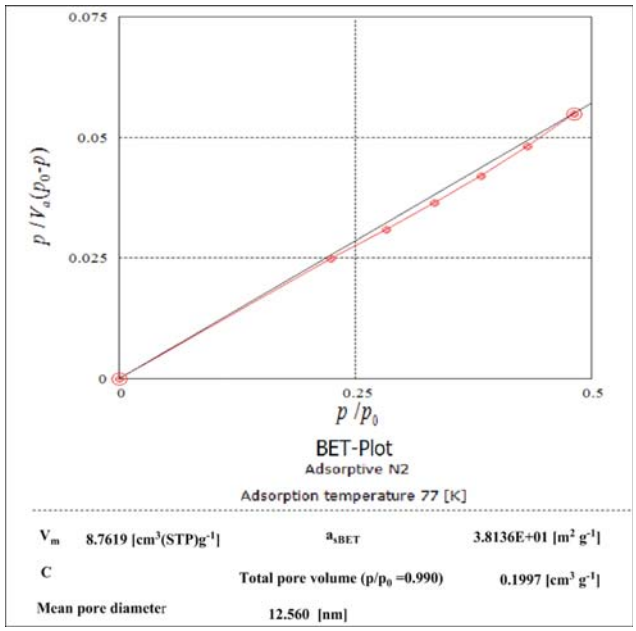

Fig. 5. BET adsorption plot of Fe_3O_4@HPEI nanoparticles.

4. BET

The specific surface area of the Fe_3O_4@HPEI nanoparticles was measured by BET (Brunauer-Emmet-Teller) analyzer. The data of BET are presented in Fig. 5. It is obvious that the Fe_3O_4@HPEI had a high specific surface area 38.13 m^2/g that is helpful to adsorption. In addition, Fe_3O_4@HPEI had a high active surface, as pore vol-

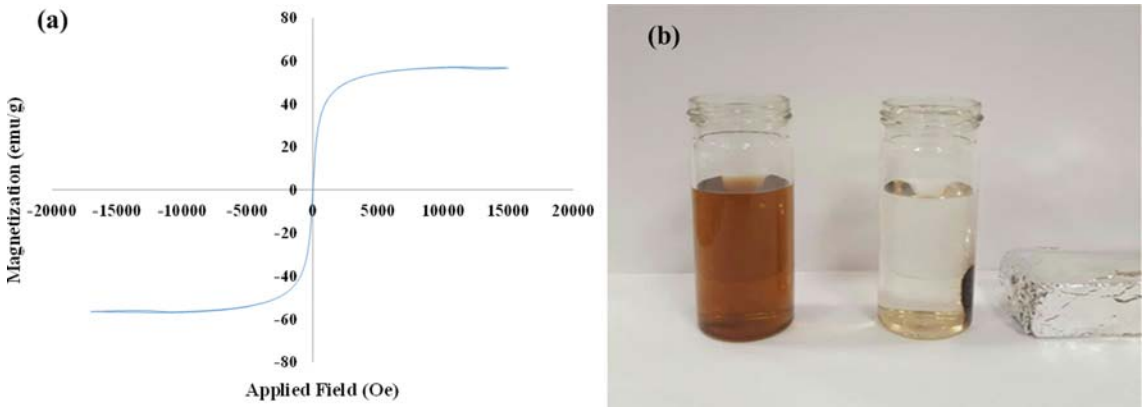

Fig. 6. (a) The diagram of VSM magnetization, and (b) the magnetic separation of Fe_3O_4@HPEI nanoparticles after HA adsorption.

Table 2. Experimental and predicted data for HA adsorption on Fe_3O_4@HPEI nanoparticles

Run number	Level of variables				Response (HA removal %)	
	HA concentration (mg/L)	pH	Time (min)	Adsorbent dose (g/L)	Experimental	Predicted
1	100	6	16	0.04	14.89	19.1
2	55	6	2	0.04	10.59	13.18
3	55	6	30	0.04	21.08	20.75
4	55	6	16	0.17	23.35	18.73
5	55	6	30	0.3	28.94	30.29
6	55	3	16	0.04	91.72	88.94
7	55	9	2	0.17	15.92	10.61
8	55	3	16	0.3	97.79	98.48
9	55	9	30	0.17	16.71	18.19
10	55	3	2	0.17	84.23	86.91
11	10	3	16	0.17	82.31	87.37
12	10	6	16	0.3	40.93	34.07
13	10	9	16	0.17	18.71	23.16
14	55	6	2	0.3	21.77	22.72
15	55	6	16	0.17	22.72	18.73
16	55	3	30	0.17	97.31	94.48
17	100	3	16	0.17	96.86	94.02
18	55	6	16	0.17	16.26	18.73
19	55	6	16	0.17	16.84	18.73
20	10	6	30	0.17	26.61	25.23
21	100	6	2	0.17	13.52	12.22
22	55	6	16	0.17	16.6	18.73
23	55	9	16	0.04	13.33	12.64
24	55	6	16	0.17	17.64	18.73
25	100	6	30	0.17	16.91	19.8
26	10	6	2	0.17	16.08	17.66
27	100	9	16	0.17	9.10	5.64
28	55	9	16	0.3	18.66	22.18
29	10	6	16	0.04	17.84	14.83
30	100	6	16	0.3	18.59	18.94

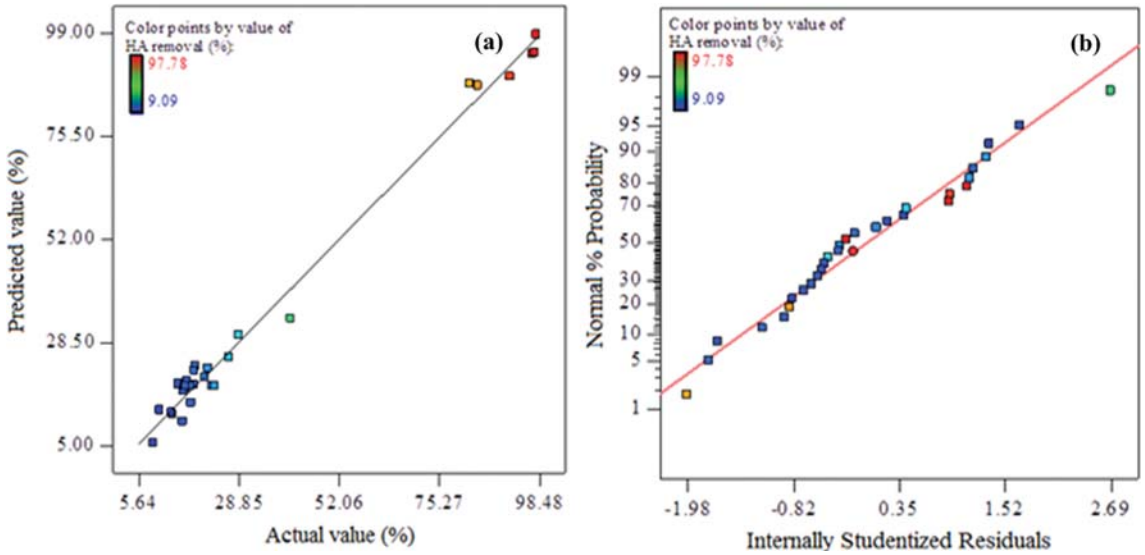

Fig. 7. (a) The plot of the experimental data against predicted data, and (b) Normal probability plot for HA adsorption on Fe_3O_4@HPEI nanoparticles.

umes and average pore diameters were 0.1197 cm^3/g and 12.56 nm, respectively. In another study, Xia et al. stated that the specific surface area of Fe_3O_4@PEI was 7.0 m^2/g [27].

5. VSM Analysis

Magnetic materials should have strong magnetic properties to be easily separated from aqueous solutions [39]. The specific saturation magnetization of Fe_3O_4@HPEI nanoparticles was assessed by a vibrating sample magnetometer (VSM). Fig. 6(a) shows the diagram of VSM magnetization. The specific saturation magnetization of the Fe_3O_4@HPEI nanoparticles was about 56.7 emu/g. According to Fig. 6(b), the modified Fe_3O_4 nanoparticles have good magnetic properties and could be easily separated from the solution by an external magnetic field.

The Fe_3O_4@HPEI nanoparticles had superparamagnetic behavior and low saturation magnetization values that can be used as a magnetic adsorbent.

6. Box-Behnken Design

Based on the Box-Behnken design, 30 runs were conducted, and the results of adsorption experiments are presented in Table 2. Table 2 and Fig. 7(a) show the experimental data and the model predictions on the HA adsorption by Fe_3O_4@HPEI nanoparticles. Fig. 7(b) illustrates the normal probability of residuals. It reveals that residual points are close to a straight line. which indicates that the error terms are definitely normal and the selected regression model is appropriate [40].

7. Multiple Regression Analysis and ANOVA

The multiple regression analysis and the accuracy of the model were analyzed by ANOVA, presented in Table 3. The model adequacy was checked by P-value, F-value, R^2, and lack of fit [41]. Based on the statistical testing of the model, P-value was less than 0.05, demonstrating the model was significant at the 95% confidence level [42]. The high F-value of 245.2 describing the model is statis-

Table 3. Results of analysis of variance (ANOVA) for HA adsorption on Fe_3O_4@HPEI nanoparticles

Source	Sum of squares	df	Mean square	F-value	p-Value
Model	26376.14	6	3297.02	245.22	<0.0001
A	88.62	1	88.62	6.59	0.018
B	17463.54	1	17463.54	1298.8	<0.0001
C	172.07	1	172.07	12.8	0.0018
D	272.94	1	272.94	20.3	0.0002
AB	145.93	1	145.93	10.85	0.0035
AD	94.09	1	94.09	7	0.0151
B^2	8134.91	1	8134.91	605.05	<0.0001
D^2	64.38	1	64.38	4.79	0.0401
Residual	282.35	21	13.45		
Lack of fit	229.86	16	14.37	1.37	0.3892
Pure error	52.49	5	10.5		
Cor total	26658.48	29			

R-squared: 0.989, Adj R-squared: 0.985, Pred R-squared: 0.968

tically acceptable [37]. And the lack of fit of the statistical model was more than 0.05, which was suitable [43]. The correlation coefficient (R^2) indicates how differences in one variable can be explained by a difference in a second variable and describes their interactions [44]. The higher R^2 value (0.989), close to 1, demonstrated the aptness of the model [45]. According to the results, the individual effects of independent parameters were significant as the corresponding P-values were less than 0.05.

The regression coefficients were estimated by using multiple regression technique. The regression model equation is given as follows:

$$\text{HA removal (\%)} = +205.699 + (0.349 \times A) - (55.35 \times B) + (0.27 \times C) + (21.749 \times D) - (0.0447 \times A \times B) - (0.829 \times A \times D) + (3.758\ B^2) + (178.041 \times D^2) \quad (4)$$

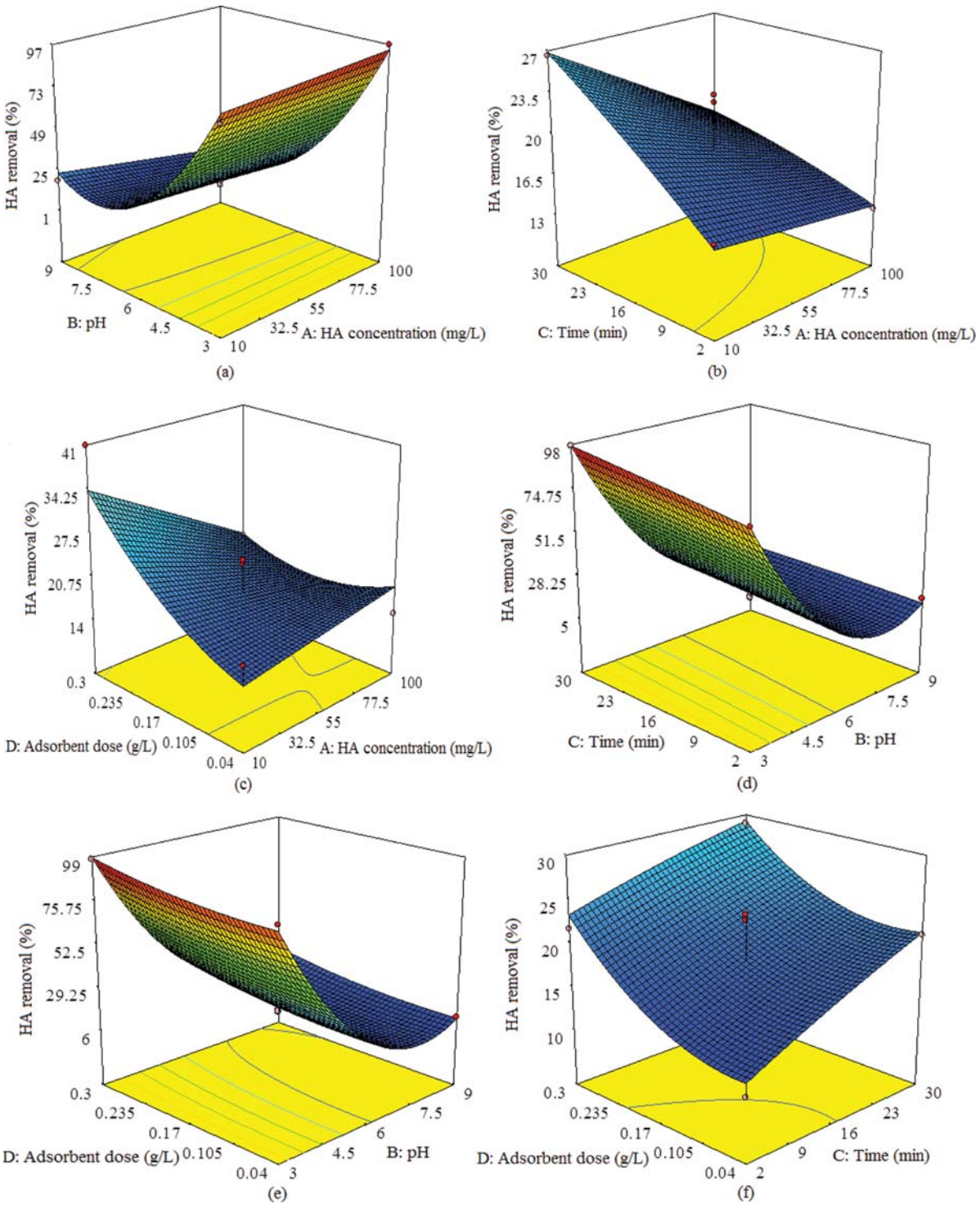

Fig. 8. The 3D surface plots for HA adsorption on the Fe_3O_4@HPEI nanoparticles.

The independent variables of HA concentration, pH, contact time, and adsorbent dose were coded as A, B, C, and D in the model, respectively. According to the coefficients in Eq. (4), the positive and negative signs of each parameter and their interaction, respectively, indicated the synergistic and adversary effects on the response. Thus, contact time, HA concentration and adsorbent dose had a synergistic effect on the HA adsorption, whereas pH had an adverse effect.

8. Interactive Effect of Parameters

Assessment of the interactive effect of parameters in a process is crucial for multivariate optimization [46]. The interactions between variables are presented in Fig. 8. According to Fig. 8(a), increasing HA concentration from 10 to 100 mg/L and decreasing pH from 9 to 3 leads to increasing the efficiency of HA adsorption. An increase in HA concentration leads to an increase in the driving forces to overcome the resisting forces in order to pass HA molecules from liquid to the adsorbent surface [47]. Similar results by Derakhshani et al. [1] and Wang et al. [48] also reported that by increasing HA concentration, adsorption capacity is also increased.

Pursuant to Fig. 8(a), (d), (e), as can be seen, the removal efficiency increased when pH decreased from 9 to 3. It is noticeable that pH played a major role in removing HA by Fe_3O_4@HPEI nanoparticles. This result may be attributed to the surface charge of Fe_3O_4@HPEI nanoparticles and the nature of HA. At lower pH, the number of H^+ ions increased and leading to the protonation of the amine groups on the Fe_3O_4@HPEI nanoparticles, which improved the positively charged surface of nanoparticles for the binding HA negatively charged [10]. Similar findings were reported by Pasandideh et al. [49] and Wang et al. [50], that maximum adsorption of HA on magnetic nanoparticles was observed at pH 3.

Contact time also plays an important role in designing the adsorption process. Based on Fig. 8(b), (d), (f), it is observed that with increasing contact time from 2 to 30 minutes the removal efficiency of HA increased. This is because of a large number of empty surface sites existing to attract HA molecules [51]. Similar results were reported by Malakootian et al. who studied on the removal of Acid green 20 by modified Sepiolite [43].

As mentioned in Fig. 8(c), (e), (f), the adsorbent dose grows from 0.04 to 0.3 g/L causing the rise of the adsorption. This could be explained due to the accessibility of rather active sites at higher mass [52]. Similar trend was reported by Fakhri et al. for antibiotic removal by MgO nanoparticles and ZnO-MgO nanocomposites [53]. Also, similar interaction for adsorption of phenol and 4-chlorophenol by spherical activated carbon was reported by Leong et al. [54].

The simultaneous influence of contact time and the adsorbent dose is presented in Fig. 8(f). As shown, at a higher dose of Fe_3O_4@HPEI nanoparticles more active sites are available for the adsorption, and longer time increases the interaction between the adsorbent and adsorbate, allowing more adsorption percentage [51].

9. Optimization

Box Behnken design provides a set of experiments, within the specified range of factors for the optimization of the adsorption process. According to the suggested statistical model, the optimal condition was acquired at the initial HA concentration 79 mg/L, adsorbent dose 0.128 g/L, pH 3 and contact time 29 min. The experimental result shows HA removed in optimum condition up to 97.27%. It was close to the response predicted by the model (95.6%), which confirmed the validity of the suggested model. Under the optimum condition, the HA adsorption capacity of Fe_3O_4@HPEI was 600 mg/g. Moreover, comparison of Fe_3O_4@HPEI nanoparticles with Fe_3O_4 for HA adsorption demonstrated Fe_3O_4 removed 8.7% of HA in optimal circumstances. It shows that the surface modification of Fe_3O_4 nanoparticle with HPEI has highly increased its capacity for HA removal.

10. Adsorption Kinetics

Adsorption kinetics have been applied to predict the adsorption rate and identify the mechanism that controls the adsorption process [55]. The pseudo-first-order model and pseudo-second-order model were utilized to investigate the mechanism of HA adsorption on Fe_3O_4@HPEI nanoparticles (Fig. 9).

The pseudo-first-order kinetic model can be expressed by Eq. (5):

$$\log(q_e - q_t) = \log q_e - \frac{k_1}{2.303}t \quad (5)$$

where q_t is the adsorption capacity at time t (min), q_e (mg/g) is the

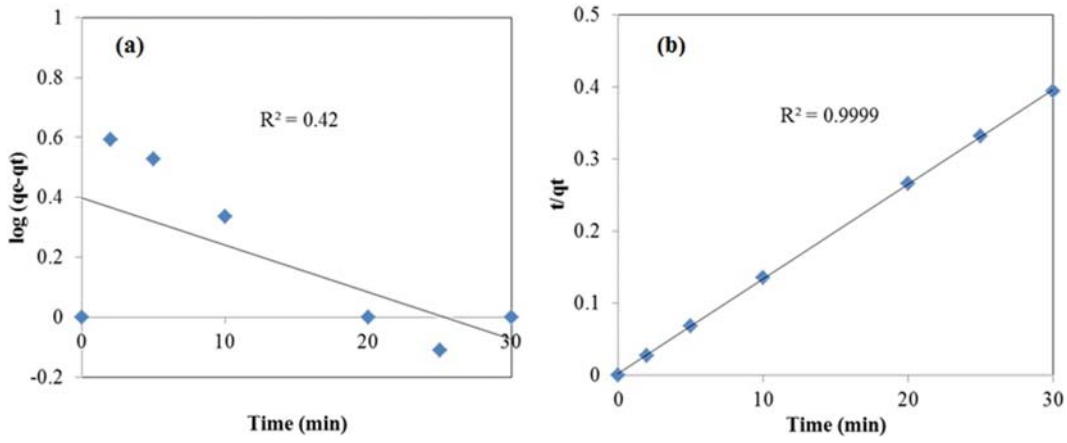

Fig. 9. (a) Pseudo-first-order, and (b) pseudo-second-order plots for HA adsorption on Fe_3O_4@HPEI nanoparticles (HA concentration: 79 mg/L, pH: 3, adsorbent dose: 0.128 g/L).

Table 4. Kinetic parameters for HA adsorption on Fe_3O_4@HPEI nanoparticles

Kinetic	Kinetic constant	Value
Pseudo-first order	q_e (mg/g)	1.49
	k_1*10^{-3} (min^{-1})	0.036
	R^2	0.42
Pseudo-second order	q_e (mg/g)	75.76
	k_2*10^{-4} (mg/g min)	0.087
	R^2	0.9999

adsorption capacity at equilibrium, k_1 (min^{-1}) is the pseudo-first-order rate constant. q_e and K_1 were computed from the slope and intercept of the plot of log ($q_e - q_t$) versus time.

The pseudo-second-order kinetic model can be described by Eq. (6) [56]:

$$\frac{t}{q_t} = \frac{1}{K_2 q_e^2} + \frac{t}{q_e} \tag{6}$$

where K_2 (mg/g min) is the pseudo-second-order rate constant. K_2 is obtained from the intercept and the plot of t/q_t versus time [57].

The parameter values of kinetic models for HA adsorption on Fe_3O_4@HPEI nanoparticles are listed in Table 4. As observed in Table 4 and Fig. 9, the correlation coefficient (R^2) of pseudo-second order (0.9999) is higher than the pseudo-first-order (0.42). This result indicates that the mechanism of HA adsorption on Fe_3O_4@HPEI belongs to the pseudo-second-order kinetic model. So the adsorption process is controlled by chemical adsorption mechanism [10].

11. Adsorption Isotherm Study

The surface properties and capacity of adsorbent are usually described by equilibrium adsorption isotherms [58]. In this study, Langmuir, Freundlich, and Dubinin-Radushkevich isotherms were employed to describe the adsorption isotherm under different humic acid concentrations. The Langmuir model linear equation was presented in Eq. (7):

$$\frac{1}{q_e} = \frac{1}{b q_{max}} + \frac{1}{q_{max}} \frac{1}{C_e} \tag{7}$$

where q_e (mg/g) is the adsorption capacity at equilibrium condition and C_e (mg/L) is HA equilibrium concentration. q_m (mg/g) is the maximum adsorption capacity and b (L/mg) is the Langmuir constant. q_m and b were determined from the intercept and slope of $1/q_e$ versus $1/C_e$ linear plot, respectively.

The Freundlich isotherm is represented by the following equation:

$$\log q_e = \log K_f + \frac{1}{n} (\log C_e) \tag{8}$$

where q_e and C_e are described above. K_f (mg/g)(L/mg)$^{1/n}$ and n are Freundlich constant and the intensity of adsorption, which can be computed from the linear plot of log q_e against log C_e.

Dubinin-Radushkevich isotherm can be used to describe adsorption mechanism with a Gaussian energy distribution onto a heterogeneous solid's surface. The linear equation form of Dubinin-

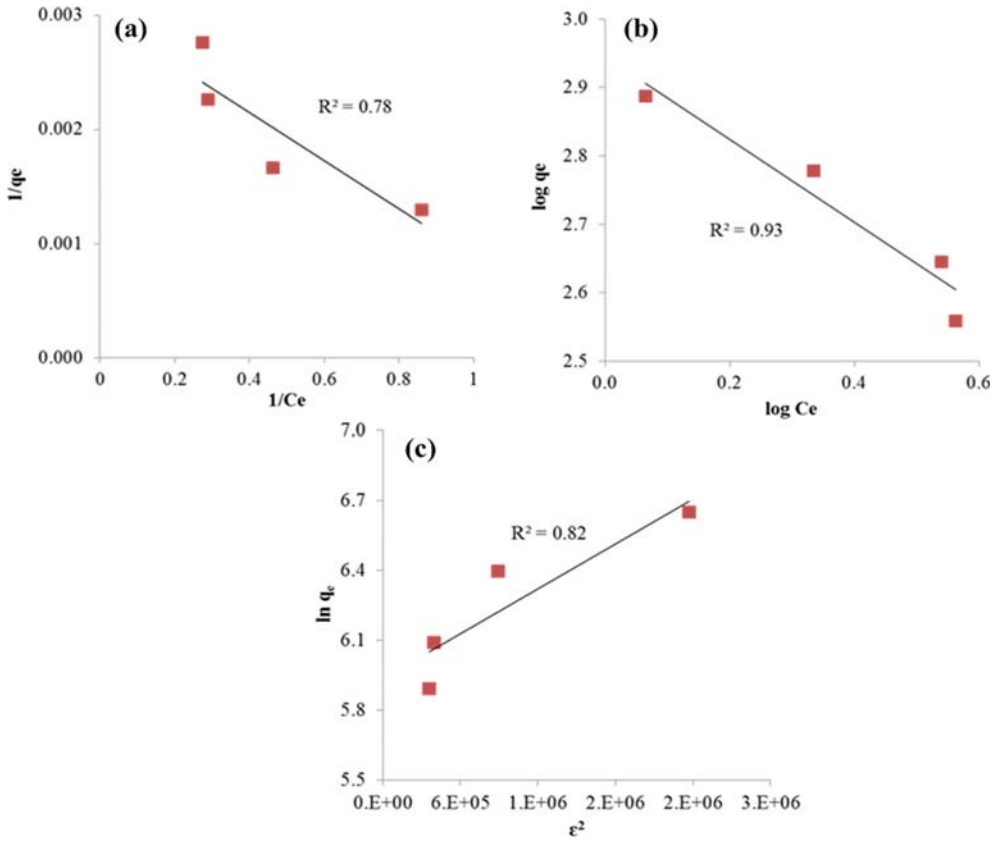

Fig. 10. (a) Langmuir, (b) Freundlich, and (c) Dubinin-Radushkevich isotherms for HA adsorption on Fe_3O_4@HPEI nanoparticles

Table 5. Isotherm parameters for HA adsorption on Fe_3O_4@HPEI nanoparticles

Adsorption isotherm	Isotherm coefficient	Value
Langmuir	q_{max} (mg/g)	476.2
	b (L/mg)	0.7
	R^2	0.78
Freundlich	K_F (mg/g)(L/mg)$^{1/n}$	879
	n	1.65
	R^2	0.93
Dubinin-Radushkevich	β (mol^2/J^2)	3*10^{-7}
	q_m (mg/g)	377.6
	R^2	0.82

Radushkevich model is given by:

$$\ln q_e = \ln q_m - \beta\varepsilon^2 \quad (9)$$

where q_m (mg/g) is the theoretical saturation capacity, β is Dubinin-Radushkevich isotherm constant related to the adsorption energy (mol^2/J^2), and ε is the Polanyi potential, which can be calculated by the following equation:

$$\varepsilon = R.T.\ln\left[1+\frac{1}{C_e}\right] \quad (10)$$

where R (J/mol K) is the gas constant, T (K) is the absolute temperature and C_e (mg/L) is adsorbate equilibrium concentration. The values of q_m and β were obtained by drawing a curve between $\ln q_e$ versus ε^2 [59].

Fig. 10 shows the Langmuir, Freundlich, and Dubinin-Radskovich isotherm models, and the isotherm parameters are presented in Table 5. As can be seen, the highest correlation coefficient (R^2= 0.93) is related to the Freundlich isotherm, which is close to 1. Therefore, the HA adsorption on the adsorbent follows the Freundlich isotherm. This result indicates that the adsorption of HA on the Fe_3O_4@HPEI surface sites is multilayer [30].

Furthermore, Table 6 shows the comparison of HA adsorption capacity by different adsorbents. It is obvious that Fe_3O_4@HPEI nanoparticles have better adsorption capacity than other adsorbents.

12. Thermodynamic Study

Thermodynamic parameters reflect the relationship between HA adsorption and temperature. Fig. 11(a) shows the effect of temperature at the range from 298 to 328 K on the HA adsorption by Fe_3O_4@HPEI nanoparticles. The adsorption thermodynamic has been investigated via thermodynamic parameters, including the standard entropy change ΔH (kJ·mol^{-1}), the average standard enthalpy ΔS (J·mol^{-1}·K^{-1}) and the change in Gibbs free energy ΔG (kJ·mol^{-1}) that calculated by the following equations:

Table 6. The comparison of maximum HA adsorption capacity of various adsorbents

Adsorbent	Maximum adsorption capacity (mg/g)	References
Palygorskite	17	[7]
HDTMA-Bentonite	330.34	[60]
Zinc oxide-coated zeolite	60	[61]
Fe_3O_4@SiO_2-PANI	36.3	[48]
Fe_3O_4@Chitosan	44.8	[47]
Fe_3O_4@PEG	59.9	[26]
Fe_3O_4@Mg/Al-LDHs	353.8	[50]
Fe_3O_4@HPEI	476.2	This work

Table 7. Thermodynamic parameters for HA adsorption on Fe_3O_4@HPEI nanoparticles

Temperature (K)	ΔG (kJ/mol)	ΔH (kJ/mol)	ΔS (J/mol K)
298	−13.94	78.3	307
308	−14.76		
318	−19.99		
328	−22.51		

$$\Delta G = -RT\ln K_d \quad (11)$$

$$\ln K_d = \frac{\Delta S}{R} - \frac{\Delta H}{RT} \quad (12)$$

$$\Delta G = \Delta H - T\Delta S \quad (13)$$

where T is temperature, and K_d and R are equilibrium distribution constant and universal gas constant (8.314 J mol^{-1} K^{-1}), respectively. The values of ΔH and ΔS (Table 7) were calculated from the slope and intercept of the plot of ln K_d versus 1/T (Fig. 11(b)) [62].

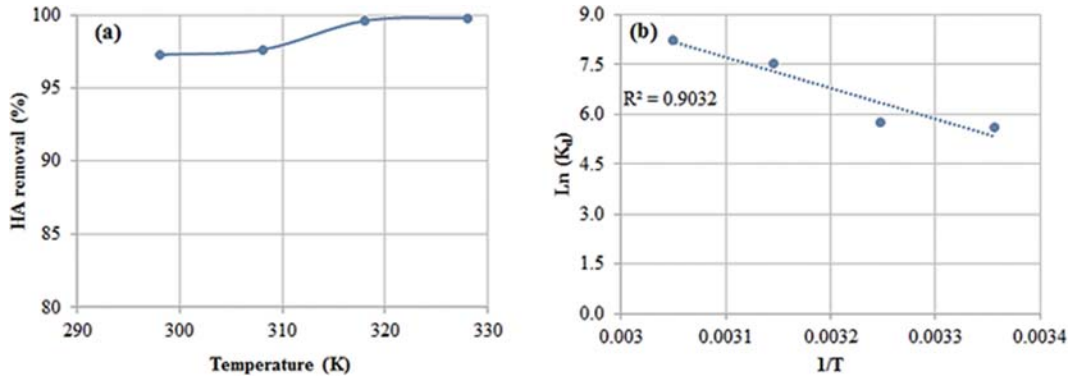

Fig. 11. (a) Effect of temperature on HA adsorption, and (b) plot of ln K_d versus 1/T.

By considering the results, the positive value of ΔH shows that the adsorption was endothermic [63], while positive ΔS indicated that the disorder of solid/liquid interface was increased throughout the adsorption process. The negative ΔG value confirmed that the sorption process was spontaneous [64].

13. Influence of Ionic Strength

Inorganic ions (Br^-, Cl^-, F^-, NO_3^-) at low concentrations naturally exist in natural waters [65], which may remarkably affect the efficiency of the adsorption process, because they can bind to functional groups on the surface of nanoparticles [66]. In the present research, the influence of the ionic strength on the HA adsorption onto Fe_3O_4@HPEI nanoparticles was investigated. So, different concentrations of NaCl from 100 to 500 mg/L were added to the solutions containing 79 mg/L HA. From the results shown in Fig. 12, it is evident that HA adsorption efficiency on Fe_3O_4@HPEI nanoparticles decreased with increasing ionic concentration of NaCl, probably since inorganic anions (Cl^-) occupy the active sites of adsorbent and compete with HA molecule for adsorption onto the adsorbent surface [50].

14. Regeneration of Fe_3O_4@HPEI

The reuse of adsorbents is a crucial factor in the practical application of the adsorbent [67]. To evaluate the reusability of the Fe_3O_4@HPEI nanoparticles, HA loaded on the Fe_3O_4@HPEI nanoparticles was desorbed by washing three times with 0.1 mol/L NaOH and deionized water. Then, the rinsed nanoparticles were subjected to HA removal again. The data in Fig. 13 show that Fe_3O_4@HPEI nanoparticles retain high HA removal efficiency, about 82.83%, after four consecutive cycles. These data confirm that Fe_3O_4@HPEI can be used frequently to remove HA with no significant reduction in its efficiency.

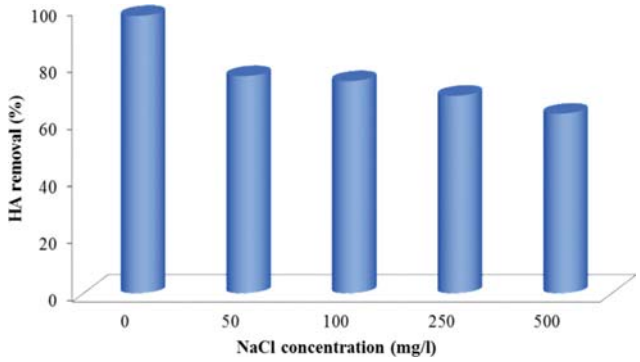

Fig. 12. Effect of NaCl concentration on HA adsorption on Fe_3O_4@HPEI nanoparticles (HA concentration: 79 mg/L, pH: 3, adsorbent dose: 0.128 g/L, time 29 min).

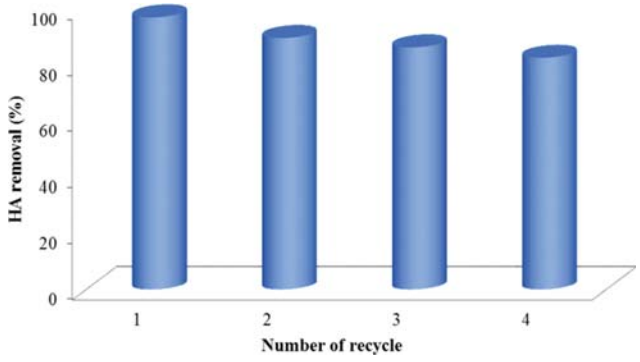

Fig. 13. Regeneration of Fe_3O_4@HPEI (HA concentration: 79 mg/L, pH: 3, adsorbent dose: 0.128 g/L, time 29 min).

CONCLUSION

The characterization of the synthesized Fe_3O_4@HPEI nanoparticles showed HPEI was successfully grafted on the surface of Fe_3O_4. The fabricated Fe_3O_4@HPEI nanoparticles could be utilized as a suitable adsorbent to remove HA from the aqueous environment. Higher HA adsorption efficiency was found when the HA concentration, adsorbent dose and contact time enhanced and the pH value was set in the acidic range. According to Box-Behnken design, the optimal condition was acquired at initial HA concentration 79 mg/L, adsorbent dose 0.128 g/L, pH 3 and contact time 29 min, which up to 97.27% HA was adsorbed by Fe_3O_4@HPEI. It was close to the predicted response by the model (95.6%) that confirmed the validity of the suggested model. The adsorption data were fitted to the pseudo-second-order kinetic and Freundlich isotherm. Thermodynamic parameters indicated that the adsorption process was spontaneous and endothermic. Moreover, the regeneration study indicated that Fe_3O_4@HPEI can be used frequently to remove HA from aqueous solution.

ACKNOWLEDGEMENT

The authors would like to thank Shahid Sadoughi University of Medical Sciences for supporting current research (Grant no: 5172).

REFERENCES

1. E. Derakhshani and A. Naghizadeh, *J. Mol. Liq.*, **259**, 76 (2018).
2. H. Wu, Z. Ai and L. Zhang, *Water Res.*, **52**, 92 (2014).
3. K. Szymański, A. W. Morawski and S. Mozia, *Korean J. Chem. Eng.*, **305**, 19 (2016).
4. M. Gong, S. Nanda, H. N. Hunter, W. Zhu, A. K. Dalai and J. A. Kozinski, *Catal. Today*, **291**, 13 (2017).
5. M. Zulfikar, I. Afrianingsih, A. Bahri, M. Nasir, A. Alni and H. Setiyanto, *J. Phys.*, **1013**, 012202 (2018).
6. H. Rezaei, M. R. Narooie, R. Khosravi, M. J. Mohammadi, H. Sharafi and H. Biglari, *Int. J. Electrochem. Sci.*, **13**, 2379 (2018).
7. M. Wang, L. Liao, X. Zhang and Z. Li, *Appl. Clay Sci.*, **67**, 164 (2012).
8. J. Liu, J. Cao, H. Chen and D. Zhou, *Colloids Surf.*, **481**, 276 (2015).
9. F. Tahmasebi, M. Alimohammadi, R. Nabizadeh, M. Khoobi, K. Karimian and A. Zarei, *Korean J. Chem. Eng.*, **36**, 894 (2019).
10. S. Li, M. He, Z. Li, D. Li and Z. Pan, *J. Mol. Liq.*, **230**, 520 (2017).
11. X. Hui, R. Jiao, F. Xiao and D. Wang, *Colloids Surf.*, **490**, 189 (2016).
12. M. Alimohammadi, M. Askari, M. Dehghani, A. Dalvand, R. Saeedi, K. Yetilmezsoy, B. Heibati and G. McKay, *Int. J. Electrochem. Sci.*, **14**, 2125 (2017).
13. A. Behjat, S. Mozaheb, M. B. Khalili, B. Vakhshour, S. H. Zare and Z. M. Falah, *Water. Wastewater.*, **18**, 60 (2007).
14. V. Shankar, J. Heo, Y. A. Al-Hamadani, C. M. Park, K. H. Chu and

Y. Yoon, *J. Environ. Manage.*, **197**, 610 (2017).
15. S. Song, S. Huang, R. Zhang, Z. Chen, T. Wen, S. Wang, T. Hayat, A. Alsaedi and X. Wang, *Chem. Eng. Trans.*, **325**, 576 (2017).
16. Z. Zhang and J. Kong, *J. Hazard. Mater.*, **193**, 325 (2011).
17. H. L. Fan, L. Li, S. F. Zhou and Y. Z. Liu, *Ceram. Int.*, **42**, 4228 (2016).
18. Q. Jiang, S. Zheng, R. Hong, S. Deng, L. Guo, R. Hu, B. Gao, M. Huang, L. Cheng and G. Liu, *Appl. Surf. Sci.*, **307**, 224 (2014).
19. P. Wang, X. Wang, S. Yu, Y. Zou, J. Wang, Z. Chen, N. S. Alharbi, A. Alsaedi, T. Hayat and Y. Chen, *Chem. Eng. J.*, **306**, 280 (2016).
20. A. A. Al-rashdi, *Anal. Chem. Res.*, **10**, 9 (2016).
21. Q. Lu, X. Dai, P. Zhang, X. Tan, Y. Zhong, C. Yao, M. Song, G. Song, Z. Zhang and G. Peng, *Int. J. Nanomed.*, **13**, 2491 (2018).
22. S. Duan, X. Xu, X. Liu, Y. Wang, T. Hayat, A. Alsaedi, Y. Meng and J. Li, *J. Colloid Interface Sci.*, **513**, 92 (2018).
23. A. Dalvand, R. Nabizadeh, M. Reza Ganjali, M. Khoobi, S. Nazmara and A. Hossein Mahvi, *J. Magn. Magn. Mater.*, **404**, 179 (2016).
24. D. Hu, X. Wan, X. Li, J. Liu and C. Zhou, *Int. J. Biol. Macromol.*, **105**, 1611 (2017).
25. A. Cahyana, D. Fitria, B. Ardiansah and D. Rahayu, *IOP Conf Ser. Mater. Sci. Eng.*, IOP Publishing, 012026 (2017).
26. M. Kumari and S. K. Gupta, *Environ. Sci. Pollut. Res.*, **25**, 25565 (2018).
27. T. Xia, Y. Guan, M. Yang, W. Xiong, N. Wang, S. Zhao and C. Guo, *Colloids Surf.*, **443**, 552 (2014).
28. B. Chen, Y. Liu, S. Chen, X. Zhao, X. Meng and X. Pan, *J. Taiwan. Iinst. Chem. Eng.*, **67**, 191 (2016).
29. Y. R. Hu, C. Guo, F. Wang, S. K. Wang, F. Pan and C. Z. Liu, *Chem. Eng. J.*, **242**, 341 (2014).
30. A. Dalvand, M. Khoobi, R. Nabizadeh, M. R. Ganjali, E. Gholibegloo and A. H. Mahvi, *J. Polym. Environ.*, **26**, 3470 (2018).
31. C. Jung, N. Phal, J. Oh, K. H. Chu, M. Jang and Y. Yoon, *J. Hazard. Mater.*, **300**, 808 (2015).
32. Z. Zaheer, A.-A. Aisha and E. S. Aazam, *J. Mol. Liq.*, **283**, 287 (2019).
33. J. Liu, N. Wang, H. Zhang and J. Baeyens, *J. Environ. Manage.*, **238**, 473 (2019).
34. S. Jafarinejad, M. Faraji, Z. Norouz and J. Mokhtari-Aliabad, *J. Water. Environ. Nanotechnol.*, **3**, 58 (2018).
35. R. A. Fallahzadeh, A. H. Mahvi, M. N. Meybodi, M. T. Ghaneian, A. Dalvand, M. H. Salmani, H. Fallahzadeh and M. H. Ehrampoush, *Korean J. Chem. Eng.*, **36**, 713 (2019).
36. N. Yousefi, R. Nabizadeh, S. Nasseri, M. Khoobi, S. Nazmara and A. H. Mahvi, *Korean J. Chem. Eng.*, **34**, 2342 (2017).
37. K. Alizadeh, E. Khaledyan and Y. Mansourpanah, *J. Water. Environ. Nanotechnol.*, **3**, 243 (2018).
38. T. Qi, C. Huang, S. Yan, X. J. Li and S. Y. Pan, *Talanta.*, **144**, 1116 (2015).
39. X. Cao, M. Wang, L. Sun, X. Ren and G. Pei, *J. Sci. Food Agric.*, **98**, 3588 (2018).
40. H. Zarei, S. Nasseri, R. Nabizadeh, F. Shemirani, A. Dalvand and A. H. Mahvi, *Desalin. Water. Treat.*, **67**, 196 (2017).
41. P. Sahoo, A. Pratap and A. Bandyopadhyay, *Int. J. Ind. Eng. Computation.*, **8**, 385 (2017).
42. E. C. Ngoe, B. Aurelien, T. T. D. Raoul and N. G. Ndifor-Angwafor, *Int. J. Res. Publ.*, **9**, 1 (2018).
43. M. Malakootian, H. Hossaini, A. Asadipour and M. Daneshkhah, *Appl. Water Sci.*, **8**, 174 (2018).
44. M. M. Momeni, D. Kahforoushan, F. Abbasi and S. Ghanbarian, *J. Environ. Manage.*, **211**, 347 (2018).
45. S. Ghafari, H. A. Aziz, M. H. Isa and A. A. Zinatizadeh, *J. Hazard. Mater.*, **163**, 650 (2009).
46. A. Mukherjee, S. Banerjee and G. Halder, *J. Adv. Res.*, **14**, 11 (2018).
47. M. A. Zulfikar, S. Afrita, D. Wahyuningrum and M. Ledyastuti, *Environ. Nanotechnol, Monit. Manage.*, **6**, 64 (2016).
48. J. Wang, L. Bi, Y. Ji, H. Ma and X. Yin, *J. Colloid Interface Sci.*, **430**, 140 (2014).
49. E. K. Pasandideh, B. Kakavandi, S. Nasseri, A. H. Mahvi, R. Nabizadeh, A. Esrafili and R. R. Kalantary, *J. Environ. Health Sci. Eng.*, **14**, 21 (2016).
50. R. X. Wang, T. Wen, X. L. Wu and A. W. Xu, *RSC Adv.*, **4**, 21802 (2014).
51. C. Dong, W. Chen and C. Liu, *Appl. Surf. Sci.*, **292**, 1067 (2014).
52. K. Kalantari, M. B. Ahmad, H. R. Fard Masoumi, K. Shameli, M. Basri and R. Khandanlou, *Int. J. Mol. Sci.*, **15**, 12913 (2014).
53. A. Fakhri and S. Behrouz, *Process Saf. Environ.*, **94**, 37 (2015).
54. K. Y. Leong, S. See, J. W. Lim, M. J. Bashir, C. A. Ng and L. Tham, *Appl. Water Sci.*, **7**, 2009 (2017).
55. H. Zheng, D. Liu, Y. Zheng, S. Liang and Z. Liu, *J. Hazard. Mater.*, **167**, 141 (2009).
56. R. P. Chicinaş, H. Bedelean, R. Stefan and A. Maicaneanu, *J. Mol. Struct.*, **1154**, 187 (2018).
57. S. Zhang, Z. Wang, H. Chen, C. Kai, M. Jiang, Q. Wang and Z. Zhou, *Appl. Surf. Sci.*, **440**, 1277 (2018).
58. V. Tafakori, R. Zadmard, F. Tabandeh, M. A. Amoozegar and G. Ahmadian, *Iran Biomed J.*, **21**, 380 (2017).
59. M. N. Rashed, A. A. E. Gad and N. M. Fathy, *Adv. J. Chem.*, **2**, 347 (2019).
60. S. Bousba, N. Bougdah, N. Messikh and P. Magri, *Phys. Chem.*, **6**, 613 (2018).
61. L. Wang, C. Han, M. N. Nadagouda and D. D. Dionysiou, *J. Hazard. Mater.*, **313**, 283 (2016).
62. S. Kamran and N. Amiri Shiri, *Chem. Methodol.*, **2**, 23 (2018).
63. S. Mohebali, D. Bastani and H. Shayesteh, *J. Mol. Struct.*, **1176**, 181 (2019).
64. I. Chaari, E. Fakhfakh, M. Medhioub and F. Jamoussi, *J. Mol. Struct.*, **1179**, 672 (2019).
65. C. Onorato, L. J. Banasiak and A. I. Schäfer, *Sep. Purif. Technol.*, **187**, 426 (2017).
66. J. Wang and S. Wang, *Chem. Eng. J.*, **334**, 1502 (2018).
67. J. Wang, S. Zheng, Y. Shao, J. Liu, Z. Xu and D. Zhu, *J. Colloid Interface Sci.*, **349**, 293 (2010).